Analysis of Water Flow under Trickle Irrigation: I. Theory and Numerical Solution

F. Lafolie, R. Guennelon, and M. Th. van Genuchten*

ABSTRACT

Estimating the size of the ponded surface area is a major source of error in modeling water movement under trickle irrigation. After reviewing available approaches and models for simulating water flow under trickle irrigation, we present a new numerical solution of the governing partial differential equations that improves the prediction of the size of the ponded area at the soil surface. A common formulation could be used for both Cartesian and axicylindrical flow geometries. The spatial operator was approximated using finite differences, and time integration was performed with an implicit method. Nonlinearity was treated by means of a fixed point iterative algorithm. The proposed model is applicable to saturated-unsaturated flow in layered soils having anisotropic hydraulic properties. Accuracy and stability of the solution are checked and comparisons made with previous numerical solutions for several trickle irrigation and other unsaturated flow problems.

INCREASED IRRIGATION EFFICIENCY, reduced water stress, ease of automation, the ability to apply fertilizers and other chemicals with irrigation water, and low economic cost are some of the factors that have contributed to the increased popularity of trickle irrigation over the last few decades (Bucks et al., 1982). Trickle irrigation is now applied to a wide variety of crops grown on soils with a broad range in soil texture, soil structure, and hydraulic properties. Notwithstanding its popularity, surprisingly little attention has been paid to estimating soil water distributions during trickle irrigation under realistic field conditions. Lack of understanding of how soil water content distributions are affected by the unsaturated soil hydraulic properties has sometimes resulted in suboptimal management and low water-use efficiency (Hillel, 1985). The shape and total volume of the wetted soil region below a trickle emitter varies widely with irrigation and soil hydraulic parameters. Using the number of drippers, the discharge rate, and the irrigation frequency as adjustable parameters, a trickle irrigation system should be designed such that the wetted soil volume matches as closely as possible the crop rooting pattern.

Soil hydraulic properties usually exhibit considerable spatial variability at the field scale. An important task in the design of a drip irrigation network is to evaluate how spatial variability affects water content distributions in the field. Particularly useful would be a sensitivity analysis which shows how deterministic soil water contents are affected by variations in relevant model parameters. One application of modeling is to find an optimal combination of irrigation and hydraulic parameters that minimizes variability problems and results in field-scale water content distributions which are as homogeneous as possible.

While much has been learned about saturated-unsaturated flow in soils under drip irrigation, a number of areas in need of further investigation remain. As pointed out by Hillel (1985), these include developing realistic methods for predicting temporal and spatial variations of soil water under drip irrigation for different crop, weather, and soil conditions (including vertically and horizontally heterogeneous soil); determining the minimal and optimal fraction of soil volume needed for various crops; assessing and controlling downward seepage and leaching rates from the root zone under drip irrigation; and adjusting water discharge rates to the soil's infiltration capacity so as to aid the infiltration of water under the drippers in fine-textured or crusted soils, particularly on sloping fields. While field experiments are important for understanding the physics of flow during trickle irrigation, the above research problems cannot be solved by experimentation only. Simulation models can help greatly in the design and analysis of field experiments, and in determining the most important processes and properties affecting the performance of a trickle irrigation system.

Mathematically, water flow under drip irrigation is essentially a three-dimensional saturated-unsaturated flow problem with a moving boundary separating the ponded and unsaturated areas of the soil surface. Determination of this transient boundary condition is a major difficulty in accurately modeling drip irrigation. Hence, the main objective of this paper is to present a numerical solution of the flow equations with a rig-

F. Lafolie and R. Guennelon, Station de Science du Sol, INRA, Domaine St-Paul, B.P. 91, 84140 Montfavet, France; M.Th. van Genuchten, USDA-ARS, U.S. Salinity Lab., 4500 Glenwood Drive, Riverside, CA 92501. Received 2 May 1988. *Corresponding author.

Published in Soil Sci. Soc. Am. J. 53:1310–1318 (1989).

orous formulation and solution of the soil surface boundary problem.

REVIEW OF PREVIOUS WORK

As compared with a relatively large number of published one-dimensional unsaturated flow models, few studies thus far have focused on trickle irrigation. Most models have been analytical or quasi-analytical, with a lesser number of numerical models. Analytical models generally involve steady-state or transient line-source or point-source infiltration problems (Philip, 1971; Raats, 1971, 1972; Warrick, 1974; Lomen and Warrick, 1974; Warrick and Lomen, 1976; Ben-Asher et al., 1978; Warrick, 1985). Wooding (1968) also gave a solution for steady-state flow from a pond, while Lockington et al. (1984) proposed a solution for point-source infiltration with ponding, but without gravity. Most analytical solutions have only limited applicability because of various assumptions, including uniform initial water contents, simplified boundary conditions, nonponding surface conditions, soil homogeneity, steady-state flow, and/or exponential relationships between the pressure head and the hydraulic conductivity to enable linearization of the Kirchhoff equation.

The first and perhaps most quoted numerical solution to the three-dimensional trickle irrigation problem was given by Brandt et al. (1971). Their finite difference model has been widely used to simulate various laboratory and field experiments. For example, Bresler et al. (1971) found good agreement between results obtained with this model and experimental data for two soils, although some discrepancies were observed at relatively high trickle application rates. Levin et al. (1979) and Mostaghimi and Mitchell (1983) used the same model to study the effects of pulsed trickle irrigations on water content distributions in two different soils. Finite difference (CSMP) solutions were used by van der Ploeg and Benecke (1974), Ragab et al. (1984) and Fletcher Armstrong and Wilson (1983). These solutions did not significantly improve the initial work of Brandt et al. (1971); treatment of the surface boundary condition was in particular less accurate. Ababou (1981) later published a finite difference model similar to the one by Brandt et al., but allowing also for root water uptake. He obtained relatively good agreement with experimental data for a sand, but less-accurate results for a loamy soil.

Brandt et al. (1971), Ababou (1981) and Ragab et al. (1984) applied Kirchhoff transformations to linearize the nonlinear Richards' equation. While Brandt et al. used tabulated hydraulic functions after smoothing with a spline function, Ababou and Ragab et al. assumed exponential relationships between the water content and the hydraulic conductivity so that an explicit relationship between the Kirchhoff variable and the pressure head could be obtained. The models of van der Ploeg and Benecke (1974) and Fletcher Armstrong and Wilson (1983) used Richards' pressure-head-based flow equation. We note that the Kirchhoff transformation is not easily applied to layered soil profiles because of the discontinuities at the interfaces.

One major problem with most numerical solutions published thus far is an inaccurate treatment of the boundary condition imposed at the soil surface. This problem may explain at least some of the discrepancies which have been observed between predictions based on previous models and experimental data for soil water contents and saturated areas at the soil surface. In this paper, we present a more rigorous solution of the soil surface boundary wetting problem.

THEORETICAL

Governing Flow Equations

In our analysis, we assume that Darcy's law applies to saturated-unsaturated flow in layered soils, that the soil is nonswelling, and that hysteresis in the soil hydraulic properties can be neglected. We allow the conductivity tensor to be anisotropic in the vertical (z) and horizontal (x,y) coordinates. However, the conductivity tensor is assumed to be isotropic horizontally. Combining Darcy's law and the continuity equation leads, then, to

$$C(\psi,z)\frac{\partial\psi}{\partial t} = \frac{\partial}{\partial x}\left[K_h(\psi,z)\frac{\partial H}{\partial x}\right] + \frac{\partial}{\partial y}\left[K_h(\psi,z)\frac{\partial H}{\partial y}\right] + \frac{\partial}{\partial z}\left[K_v(\psi,z)\frac{\partial H}{\partial z}\right] \quad [1]$$

in which ψ is the soil-water pressure head (L); $H = \psi - z$ is the total head (L); C is the soil-water capacity (L^{-1}), approximated by the slope of the soil-water retention curve, $\theta(\psi)$; θ is the volumetric water content; K_h and K_v are the horizontal and vertical components of the conductivity tensor (LT^{-1}), respectively; t is time (T); z is distance (L), considered to be positive downwards; and x and y are coordinates in the horizontal plane (L). Rather than using the pressure head, ψ, we found it more convenient to work with the total head, H. Using $H = \psi - z$ and noting that $\partial\psi/\partial t = \partial H/\partial t$, Eq. [1] becomes

$$C(\psi,z)\frac{\partial H}{\partial t} = \frac{\partial}{\partial x}\left[K_h(\psi,z)\frac{\partial H}{\partial x}\right] + \frac{\partial}{\partial y}\left[K_h(\psi,z)\frac{\partial H}{\partial y}\right] + \frac{\partial}{\partial z}\left[K_v(\psi,z)\frac{\partial H}{\partial z}\right]. \quad [2]$$

Trickle irrigation may lead to two possible flow geometries: plane symmetry for a line-source system, and axicylindrical symmetry for an isolated point source. Axicylindrical symmetry holds as long as there is no interaction between neighboring point sources, while plane symmetry may always be invoked between two neighboring line sources. The flow equation for plane symmetry reduces to

$$C(\psi,z)\frac{\partial H}{\partial t} = \frac{\partial}{\partial x}\left[K_h(\psi,z)\frac{\partial H}{\partial x}\right] + \frac{\partial}{\partial z}\left[K_v(\psi,z)\frac{\partial H}{\partial z}\right] \quad [3]$$

with $(x,z) \in \Omega = [0,X] \times [0,Z]$, and for cylindrical symmetry to

$$C(\psi,z)\frac{\partial H}{\partial t} = \frac{\partial}{\partial r}\left[K_h(\psi,z)\frac{\partial H}{\partial r}\right] + \frac{\partial}{\partial z}\left[K_v(\psi,z)\frac{\partial H}{\partial z}\right] + \frac{K_h(\psi,z)}{r}\frac{\partial H}{\partial r} \quad [4]$$

with $(r,z) \in [0,R] \times [0,Z]$ in which r is the radial coordinate (Fig. 1). Notice that Eq. [3] and [4] are defined on only half of the real domain. Equation [4] can be simplified by the substitutions

$$c(\psi,z,r) = rC(\psi,z) \qquad k_{h,v}(\psi,z,r) = rK_{h,v}(\psi,z). \quad [5a,b]$$

Which leads to the following equation for cylindrical symmetry

$$c(\psi,z)\frac{\partial H}{\partial t} = \frac{\partial}{\partial r}\left[k_h(\psi,z,r)\frac{\partial H}{\partial r}\right] + \frac{\partial}{\partial z}\left[k_v(\psi,z,r)\frac{\partial H}{\partial z}\right]. \quad [6]$$

Equation [3] and [6] are now both of the type

$$C\frac{\partial H}{\partial t} = \nabla\cdot(K\nabla H)$$

and differ only because of the different forms of the "effective" soil water capacity and hydraulic conductivity coeffi-

cients C and K. Hence, the same numerical algorithm and discretization can be used for both geometries.

Initial and Boundary Conditions

The general initial condition is

$$H(r,z,t)|_{t=0} = \psi_0(z,r) - z\,. \qquad [7]$$

Because of symmetry (Fig. 1) we have a no-flow condition on boundary Γ_1, i.e.,

$$\frac{\partial \psi}{\partial r}\Big|_{r=0} = \frac{\partial H}{\partial r}\Big|_{r=0} = 0\,. \qquad [8]$$

A no-flow condition also applies to boundary Γ_2

$$\frac{\partial \psi}{\partial r}\Big|_{r=R} = \frac{\partial H}{\partial r}\Big|_{r=R} = 0\,. \qquad [9]$$

While Eq. [9] is valid without restriction for plane symmetry, the condition may not hold for cylindrical geometry if changes occur along that boundary during the calculations. The problem becomes then fully three-dimensional and the assumption of having axicylindrical symmetry can no longer be invoked to reduce the three-dimensional problem to the set of equations given above.

Three different conditions may be imposed along the bottom boundary (Γ_3) of the soil profile. If a water table is present at a depth Z, then a Dirichlet type boundary condition applies

$$H(r,Z,t) = -Z \qquad [10]$$

A free-draining profile results when the condition

$$\frac{\partial \psi}{\partial z}\Big|_{z=Z} = 0 \text{ or } \frac{\partial H}{\partial z}\Big|_{z=Z} = -1 \qquad [11]$$

is imposed. Finally the presence of an impervious layer at Z is simulated with a no-flow boundary condition

$$\frac{\partial T}{\partial z}\Big|_{z=Z} = 0\,. \qquad [12]$$

At the soil surface, we must account for interactions between the applied trickle rate, evaporation, and infiltration into the soil. The following condition holds when the soil surface remains unsaturated (no ponding)

$$Q = -K_v(\psi,r,z)\frac{\partial H}{\partial z}\Big|_{z=0} \qquad [13]$$

where $Q = Q_0/S - E$, Q_0 is the trickle discharge rate, E is the evaporation rate from the ponded area, and S is a small area over which Q is evenly distributed. However, when the applied flow rate exceeds the soil's infiltration capacity, a saturated area develops on the soil surface below the emitter. This ponded area is assumed to be circular for axicylindrical symmetry and an infinite strip for plane symmetry. We assume that there is no storage of water on the soil surface during ponding. The following Dirichlet condition then applies to the saturated zone

$$H(r,0,t) = 0 \qquad r\epsilon[0,R_s(t)] \qquad [14]$$

where $R_s(t)$ is the radius of the ponded circular area (point source) or the half-width of the strip (line source). Evaporation from the remaining part of the soil surface is described with a Neuman-type boundary condition of the form

$$-K_v(\psi,r,z)\frac{\partial H}{\partial z}\Big|_{z=0} = \begin{cases} -E_p & \psi \geq \psi_{lim} \\ 0 & \psi < \psi_{lim} \end{cases} \qquad [15]$$

where ψ_{lim} is some arbitrary lower limit of ψ, and E_p is the potential evaporation rate. The main, and significant, problem remaining is to quantify $R_s(t)$. This is discussed next.

Determination of the Ponded Area

Let $q(r,t)$ denote the distribution of vertical fluxes across the saturated zone at the soil surface. We define for both symmetries $Q_{sat}(t)$ as the total amount of water crossing the saturated zone per unit time, i.e.,

$$Q_{sat}(t) = 2\pi \int_0^{R_s} rq(r,t)\,dr \text{ (cylindrical)} \qquad [16a]$$

$$Q_{sat}(t) = 2\int_0^{R_s} q(r,t)\,dr \text{ (Cartesian)}\,. \qquad [16b]$$

Evaporation from the saturated area is assumed to occur at its potential rate, E_p, so that we can write

$$Q_{sat}(t) + \pi R_s^2(t)E_p = Q_0 \text{ (cylindrical)} \qquad [17a]$$

$$Q_{sat}(t) + 2R_s(t)E_p = Q_0 \text{ (Cartesian)}\,. \qquad [17b]$$

For notational convenience below, we drop the explicit time dependence of Q_{sat} and R_s. Combining Eq. [16] and [17] gives

$$2\pi\int_0^{R_s} rq(r,t)\,dr = Q_0 - \pi R_s^2 E_p \text{ (cylindrical)} \qquad [18a]$$

$$2\int_0^{R_s} q(r,t)\,dr = Q_0 - 2R_s E_p \text{ (Cartesian)} \qquad [18b]$$

where $q(r,t)$ is given by Darcy's law as

$$q(r,t) = -K_{v,s}\frac{\partial H}{\partial z}(r,0,t)\,. \qquad [19]$$

The time derivatives of Eq. [18a,b] are

$$-2\pi E_p R_s \frac{dR_s}{dt} = 2\pi E_p R_s \frac{dR_s}{dt} q(R_s,t) + 2\pi\int_0^{R_s} r\frac{\partial q}{\partial t}(r,t)dr \text{ (cylindrical)} \qquad [20a]$$

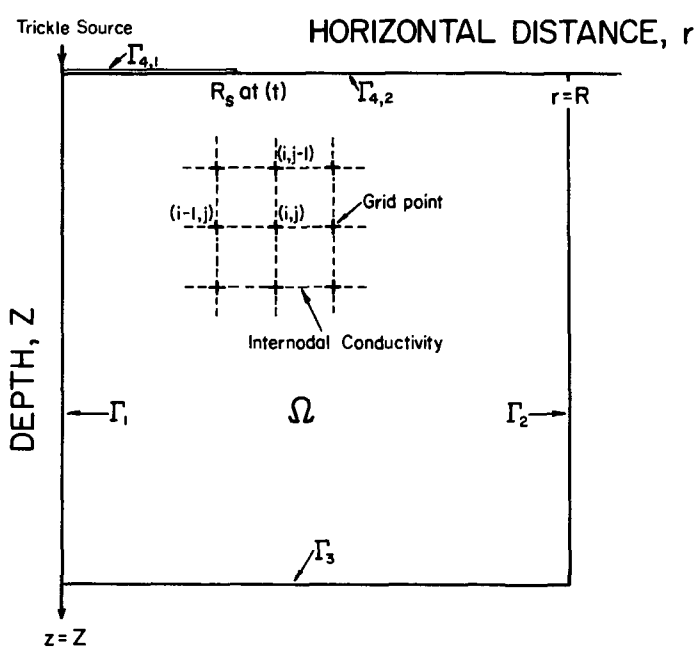

Fig. 1. Schematic cross section of the flow domain and the imposed finite difference grid system for simulating trickle irrigation.

$$-E_p\frac{dR_s}{dt} = \frac{dR_s}{dt}\,q(R_s,t) + \int_0^{R_s}\frac{\partial q}{\partial t}(rt)dr \text{ (Cartesian)} \quad [20b]$$

which leads to the differential equations

$$-R_s\frac{dR_s}{dt}[E_p + q(R_s,t)] = \int_0^{R_s} r\frac{\partial q}{\partial t}(r,t)dr \text{ (cylindrical)} \quad [21a]$$

$$\frac{dR_s}{dt}[E_p + q(R_s,t)] = \int_0^{R_s}\frac{\partial q}{\partial t}(r,t)dr \text{ (Cartesian)}. \quad [21b]$$

Equation [21a,b] shows that a decrease in the flux through the saturated zone ($\partial q/\partial t < 0$) results in an increase of the saturated area at the surface ($dR_s/dt > 0$). The initial condition for Eq. [21a,b] is the radius $R_{s,0}$ of the saturated area corresponding to the impact of a single drop. This area is numerically approximated by the area S corresponding to the first node of the finite difference grid. If we denote t_p as the time at which ponding occurs, the initial condition becomes

$$R_s(t_p) = R_{s,0}. \quad [22]$$

Thus, we obtain a set of equations describing saturated-unsaturated flow in the soil, and a differential equation predicting the evolution of R_s as a function of time. The resulting Stefan-type problem can be solved using an iterative algorithm (Mitchell and Griffith, 1980) involving alternate solutions of the flow equation, Eq. [6], and Eq. [21a,b] for R_s until convergence is reached. Two problems remain. First, accurate imposition of a Dirichlet boundary condition on $[0,R_s(t)]$ requires modification of the finite difference grid system each time a new estimate for $R_s(t)$ is obtained. This implies a need to interpolate the potential field each time a new grid is defined, with the likelihood of introducing additional errors. Also, a good approximation of the function $q(r,t)$ over the interval $[0,R_s(t)]$ is crucial for accurately solving Eq. [21]. The standard method for estimating water fluxes through the saturated zone is to use Eq. [19] in which the gradient $(\partial H/\partial z)$ is approximated with a two- or three-point uncentered scheme (Bresler et al., 1971; van der Ploeg and Benecke, 1974; Ababou, 1981; Ragab et al., 1984) according to

$$\frac{\Delta H}{\Delta z} = \frac{H_2 - H_1}{\Delta z} \quad [23]$$

$$\frac{\Delta H}{\Delta z} = \frac{-3H_1 + 4H_2 - H_3}{2\Delta z} \quad [24]$$

where H_1, H_2, and H_3 are the total head values at the first three finite difference nodes along a vertical starting from the soil surface.

Numerical experiments using two types of soils were carried out to investigate the accuracy of Eq. [24a,b] in approximating $q(r,t)$. Unacceptable errors appeared, especially with relatively large step sizes, Δz, and/or low initial water contents. These results may explain why, for coarse-textured soils where small ponded areas and very small gradients near the surface prevail, most models give relatively good results, and why, for fine-textured soils, they fail to accurately predict the ponded area on the soil surface. Hence, previous models often led to inaccurate water-content distributions in the profile, and also exhibited relatively large mass balance errors when used on fine-textured soils. A more accurate procedure for estimating $R_s(t)$ is described below.

An Alternative Method for Estimating $R_s(t)$

For any part of ω of the wetted domain (Fig. 2), we can write the mass conservation equation

$$\int_\omega \frac{d\theta}{dt}\,d\omega = -\int_\omega \text{div}(\vec{\mathbf{f}})d\omega \quad [25]$$

where $\vec{\mathbf{f}} = [K]\vec{\mathbf{Grad}}(H)$, and [K] is the conductivity tensor. The divergence theorem states that

$$\int_\omega \text{div}(\vec{\mathbf{f}})\,d\omega = \int_{\partial\omega} \vec{\mathbf{f}}\cdot\vec{\mathbf{n}}\,d\gamma \quad [26]$$

where $\vec{\mathbf{n}}$ is the outward direction normal to $\partial\omega$. Equation [26] can be expanded to give the following equation relating water content variations in ω to the various boundary fluxes

$$\int_\omega \frac{d\theta}{dt}\,d\omega = -\int_{\partial\omega}\vec{\mathbf{f}}\cdot\vec{\mathbf{n}}d\gamma = -\int_{\partial F}\vec{\mathbf{f}}\cdot\vec{\mathbf{n}}d\gamma + \int_H \vec{\mathbf{f}}\cdot\vec{\mathbf{k}}d\gamma + \int_V \vec{\mathbf{f}}\cdot\vec{\mathbf{i}}d\gamma \quad [27]$$

where $\vec{\mathbf{k}}$ and $\vec{\mathbf{i}}$ are unit vectors for the z and r coordinates, respectively; $H = [0,R_s]$, $V = [0,Z_f]$ and ∂F is an arbitrary curve inside Ω joining the points $(R_s,0)$ and $0,Z_f)$. The last integral of Eq. [27] is zero because of a no-flow boundary condition on Γ_1. Rearranging Eq. [27] gives then

$$\int_0^{R_s}\vec{\mathbf{f}}\cdot\vec{\mathbf{k}}\,dx = \int_\omega\frac{d\theta}{dt}\,d\omega + \int_{\partial F}\vec{\mathbf{f}}\cdot\vec{\mathbf{n}}\,d\gamma. \quad [28]$$

Hence, the discharge rate through the saturated zone (left-hand side of Eq. [28]) can be calculated from the rate of change in total water content in ω, and the flux through some internal boundary ∂F. For cylindrical symmetry, this boundary is generated by rotating ∂F around the axis $(0,\vec{\mathbf{k}})$, and for plane symmetry by translating ∂F along a direction orthogonal to the plane $(0,\vec{\mathbf{i}},\vec{\mathbf{k}})$. Note that when θ in ω does not change with time (steady flow in ω), the discharge rates through the saturated zone and ∂F must be equal.

We required ∂F to be such that the integration of θ over ω, as well as the estimation of the fluxes through ∂F, would be as accurate as possible. For convenience, ∂F was defined

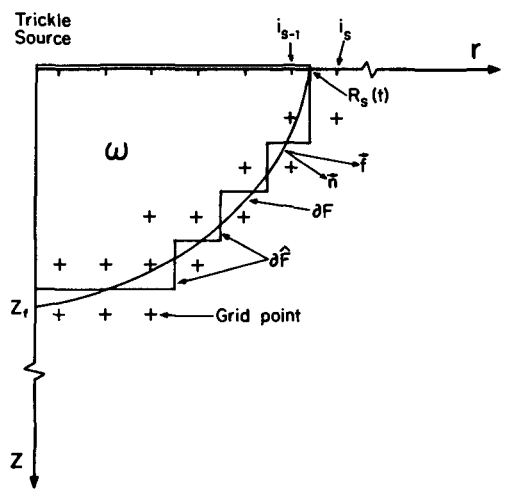

Fig. 2. Approximation of the smooth curve, ∂F, by a broken line, $\hat{\partial F}$, along the finite difference grid system.

such that the pressure head in ω was greater than some preset limit close to saturation (e.g., a few centimeters pressure head), thus guaranteeing a smoothly changing potential field. Numerical implementation of this algorithm was facilitated by approximating the original smooth boundary, ∂F, with a broken line, $\partial \hat{F}$, that follows the grid system as shown in Fig. 2. This approximation does not lead to additional errors since the divergence theorem holds for any piecewise continuous boundary. Our numerical algorithm automatically constructs the curve $\partial \hat{F}$, calculates the required fluxes, and evaluates the total moisture change in ω.

The computer algorithm to implement the above scheme is described schematically in Table 1. In this table, I_{sat} indicates the set of nodes belonging to ω, while the expression "calculate the horizontal flux through (i_f, j_f)" means to calculate the flux from node (i_f, j_f) to node $(i_f + 1, j_f)$. Similarly, "calculate the vertical flux through (i_f, j_f)" means to calculate the flux from node (i_f, j_f) to node $(i_f, j_f + 1)$. Two-point centered finite difference equations were used to calculate all fluxes through $\partial \hat{F}$.

The accuracy of the method for both symmetries was verified by simulating two-dimensional infiltration through a fixed wetted zone using several application rates. The accuracy during each time step (Δt) was expressed by the relative mass balance variable

$$R_m = \frac{V_r + \delta\theta}{V_t} \qquad [29]$$

where V_t is the amount of water applied to the soil surface during Δt, and

$$\delta\theta = \int_\omega d\theta(x,y)\, dxdy \qquad V_r = \int_{\partial F} \vec{Q}\cdot\vec{n}\, d\gamma$$

in which $d\theta$ is the local water content change during Δt, and $\vec{Q}$ is the flux through ∂F as given by Darcy's law. The variables $\delta\theta$ and V_r represent the change in water storage in ω and the flux through the boundary ∂F, respectively. For several soils and application rates, we always found the ratio R_m to be between 0.995 and 1.005. Cumulative mass balances errors during the simulations generally also remained less than 0.5%.

Discharge rates through the saturated zone calculated in this fashion take advantage of the accuracy of space-centered approximations in a region where the pressure head always varies smoothly. Also, the saturated hydraulic conductivity (K_s) is not needed to calculate hydraulic fluxes through the ponded area on the soil surface. Actually, fluxes are calculated using conductivities, which often are one to three orders of magnitude smaller than K_s, thus further reducing errors when gradients are approximated by discrete equations.

Some authors (e.g., Bresler et al., 1971; Ragab et al., 1984) have pointed out that poor estimates of K_s could have caused their deviations between calculated and experimental data. The K_s is known to be a highly variable parameter in the field, with variations of two orders of magnitude or more not being uncommon in the same field (e.g., Russo and Bresler, 1980). Hence, if one is interested in evaluating the effects of spatial variability in K_s on soil water distributions, then a model should be used in which numerical errors are not very sensitive to this parameter. Previous models may well have induced large errors in this respect. Because the hydraulic conductivity at small negative values of ψ is often an order of magnitude less than at saturation, and usually also exhibits less variability at the field scale, our approach should be more reliable than previous models.

Finally, we note that it is not necessary to obtain $R_s(t)$ as a continuous function of t. It is much simpler and more economical to use a step function $R_s'(t)$ which approaches $R_s(t)$ such that $R_s'(t)$ always coincides with a finite difference nodal point at the soil surface. For cylindrical geometry, $R_s(t)$ is then given by

$$R_s(t) = R_s'(t)\sqrt{Q_s(t)/Q_0} \qquad [30]$$

where $R_s'(t)$ is the current estimate of $R_s(t)$, and $Q_s(t)$ is the flux through the saturated area corresponding to $R_s'(t)$. If we apply boundary condition Eq. [14] to the saturated area $[0,R_s'(t)]$ rather than to $[0,R_s(t)]$, a difference, $D(t)$, between the amount of water applied and the amount entering the soil profile will result. This difference is given by $D(t) = Q_0 - Q_s(t)$. To account for $D(t)$ in the model, a flux boundary condition is imposed on the first unsaturated node, i_s, of the grid system (Fig. 2). This gives

$$Q_r(t) = -K_v(\psi,r,0)\left.\frac{\partial H}{\partial z}\right|_{z=0} \qquad [31]$$

which ensures a correct mass balance. In Eq. [31], $Q_r(t)$ is the residual flux applied at surface node i_s, and given by $Q_r(t) = D(t)/S_{is}$, where S_{is} is the soil surface area between nodes i_{s-1} and i_s of the finite difference grid. As the infiltration rate through the saturated zone decreases, the residual flux, $Q_r(t)$, increases until saturation is reached, at which time $R_s'(t)$ jumps from node $i_s - 1$ to node i_s.

Table 1. Algorithm for calculating the curve ∂F and the flux through the unsaturated zone at the soil surface.

Algorithm
a. Initialize $(i_f,j_f) = (i_s,1)$ where (i_s) is the first unsaturated node at the top of the soil (see Fig. 2).
b. Calculate the horizontal flux between the nodes $(i_f - 1, j_f)$ and (i_f,j_f).
c. Let $(i_f,j_f) = (i_f,j_f + 1)$,
1. If $(i_f,j_f) \in I_{sat}$ then
α) Let $(i_f,j_f) = (i_f - 1,j_f)$
β) If $(i_f < 0)$ stop.
γ) If $(i_f,j_f) \in I_{sat}$ then
—calculate the vertical flux through $(i_f + 1,j_f - 1)$,
—calculate the horizontal flux through (i_f,j_f),
—go to c.
δ) If $(i_f,j_f) \notin I_{sat}$ or if $(i_f = 0)$ then
—calculate the vertical flux through $(i_f + 1,j_f - 1)$,
—let $(i_f,j_f) = (i_f,j_f - 1)$,
—go to c.

NUMERICAL APPROXIMATION OF THE FLOW EQUATION

The flow domain (Fig. 1) is divided into an unequally spaced, rectangular finite difference grid $\Omega_h = (r_1, \ldots, r_{nx}) \times (z_1, \ldots, z_{nz})$ with arbitrary node (i,j) located at (r_i,z_j). Another set of points in Ω is defined by

$$\Omega_h' = (r_1', \ldots, r_{nx+1}') \times (z_1', \ldots, z_{nz+1}') \qquad [32a]$$

such that

$$r_i' = (r_i + r_{i-1})/2 \quad i = 2,nx \qquad [32b]$$

$$z_j' = (z_j + z_{j-1})/2 \quad j = 2,nz\,. \qquad [32c]$$

To more easily include no-flow boundary conditions, we choose r_1 and r_{nx} such that $r_1' = 0$ and $r_{nx+1}' = R$. For the horizontal boundaries, Γ_3 and Γ_4, we have $z_1 = 0$ and $z_{nz} = Z$ so that $z_1' = -z_2$ and $z_{nz+1}' = 2z_{nz} - z_{nz}'$. The continuous function $H(r,z,t)$ is approximated on the finite difference grid by the time-dependent vector $[H_{i,j}]$.

Approximation of Spatial Derivatives

At any point (i,j), spatial derivatives are approximated with three-point centered finite difference equations as follows

$$\frac{\partial}{\partial r}\left(K_h\frac{\partial H}{\partial r}\right) \simeq \frac{1}{r'_{i+1} - r'_i}\left[\frac{H_{i+1,j} - H_{i,j}}{r_{i+1} - r_i}\,k_h(r'_{i+1},z_j) - \frac{H_{i,j} - H_{i-1,j}}{r_i - r_{i-1}}\,k_h(r'_i,z_j)\right]$$

$$\frac{\partial}{\partial z}\left(K_v\frac{\partial H}{\partial z}\right) \simeq \frac{1}{z'_{j+1} - z'_j}\left[\frac{H_{i,j+1} - H_{i,j}}{z_{j+1} - z_j}\,k_v(r_i,z'_{j+1}) - \frac{H_{i,j} - H_{i,j-1}}{z_j - z_{j-1}}\,k_v(r_i,z'_j)\right] \quad [33]$$

which yield a spatial approximation of quadratic order (Godounov, 1973). Internodal conductivities, k_h and k_v, are calculated by geometric means (Vauclin et al., 1979), to give

$$k_h(r'_{i+1},z_j) = [k_h(r_{i+1},z_j)k_h(r_i,z_j)]^{1/2}$$
$$k_v(r_i,z'_{j+1}) = [k_v(r_i,z_{j+1})k_v(r_i,z_j)]^{1/2}.$$

Neuman-type boundary conditions were readily included by two-point centered approximations, while Dirichlet-type nodes were directly eliminated from the final matrix equations. Flux conditions on Γ_3 and Γ_4 required virtual nodes outside the domain; these nodes give contributions that cancel with approximations from inside the domain. Combining the different spatial approximations ultimately leads to the following set of nonlinear differential equations

$$[C(H)]\left\{\frac{dH}{dt}\right\} = -[K(H)]\{H\} + \{S(H)\} \quad [34]$$

in which $[C]$ is the diagonal matrix of nodal soil water capacities, $[K(H)]$ is a multidiagonal matrix associated with the spatial derivatives, $\{S(H)\}$ is a constraint vector accounting for Neuman-type boundary conditions, and $\{dH/dt\}$ is the vector of temporal pressure derivatives at the grid nodes.

Integration in Time

Equation [34] was integrated by means of a one-step A(α)-stable method (Richtmeyer and Morton, 1967). For a differential equation of the form $y'(t) = f(y,t)$ this results in the following scheme

$$y_{j+1} = y_j + \Delta t[\alpha f(y_{j+1},t_{j+1}) + (1 - \alpha)f(y_j,t_j)] \quad [35]$$

where the indices j and $j+1$ refer to the old and new time levels, respectively. For α equal to 1/2 and 1, the well-known Crank-Nicholson and fully implicit schemes result. Applying Eq. [35] to Eq. [34] leads to

$$([I] + \alpha\Delta t[C^{-1}]^{j+1}[K]^{j+1})\{H\}^{j+1} = \alpha\Delta t[C^{-1}]^{j+1}\{S\}^{j+1} + [[I] - (1 - \alpha)\Delta t[C^{-1}]^j[K]^j]\{H\}^j + (1 - \alpha)\Delta t[C^{-1}]^j\{H\}^j \quad [36]$$

where $[I]$ is the identity matrix. The nonlinearity of this set of equations is treated by means of a fixed-point algorithm. The iterative process continues until the following criterion is satisfied

$$\|\{H\}_{k+1}^{j+1} - \{H\}_k^{j+1}\|_\infty < \epsilon \quad [37]$$

where k is the fixed-point iteration index and ϵ an error limit. Numerical tests showed that a value of 0.1 cm for ϵ was adequate; results generally changed little for ϵ-values ranging from 0.1 to 0.001. The above algorithm was also used to control the time step Δt during the calculations. The Δt was increased if the number of iterations during the preceding step was less than three, remained the same if the number of iterations was three, four or five, and was reduced for more than five iterations. The final set of linear equations is of relatively large size, and direct inversion methods can be quite time consuming. Because of the block-diagonal properties of the matrix $[K]$, the system is well suited for iterative equation solvers such as the Gauss-Seidel or SOR algorithms. We used the Gauss-Seidel method with a relative stopping criterion of 10^{-5}.

NUMERICAL VERIFICATION

Convergence and stability of the numerical solution were first studied by using increasingly smaller time (Δt) and spatial (Δr,Δz) increments and assuming a fully implicit integration in time ($\alpha = 1$). By letting Δz and Δr go to zero, simulations showed that convergence to the exact solution was quadratic everywhere in the domain, provided that Δz and Δr near the wetting front were relatively small. As expected, the fully implicit scheme showed a linear rate of convergence with Δt. We successfully used a Richardson-type extrapolation to the limit (Fairweather, 1978) with a geometric series of time increments: $\Delta t/2^i$, $i = 0,1\ldots$ Thus, we concluded that the numerical scheme was stable and convergent in space and time.

Partial verification of the numerical scheme could have also been carried out against available analytical solutions for point sources (Warrick, 1974; Lomen and Warrick, 1974), or strip and disc sources (Warrick and Lomen, 1976). Unfortunately, these solutions are for the quasi-linear Kirchhoff equation

$$\frac{\partial U}{\partial t} = \frac{k}{\beta}\Delta U - k\frac{\partial U}{\partial z}$$

in which U is the matric flux potential, and k and β are constants such that $K = K_s \exp(\beta\psi)$ and $dK/d\theta = k$. Because linearized solutions do not provide a convincing numerical check of the complete nonlinear model, we decided to compare our results with previously published solutions on problems involving both Dirichlet (Example 1) and flux-type (Example 2) boundary conditions. Several trickle irrigation problems are discussed under Example 3.

Example 1. To verify the model for Dirichlet-type conditions, we simulated the problem of infiltration from an equally spaced furrow irrigation system. The flow domain and boundary conditions are shown in Fig. 3. The problem was solved previously by Zyvoloski et al. (1976) using a finite element method, by Caussade et al. (1973) using an iterative linear/nonlinear finite difference approximation after application of Kirchhoff's transformation, and by Selim and Kirkham (1973) and Firdaouss and Ta-Phuc-Loc (1983) using alternating-direction implicit (ADI) methods with and without iteration, respectively. We refer to the studies of Zyvoloski et al. (1976) or Caussade et al. (1979) for detailed descriptions of the hydraulic properties. In our calculations, we used a regular finite difference grid with vertical and horizontal nodal spacings of 2 cm. Figure 4 compares our calculated water content distribution after 50 min of infiltration

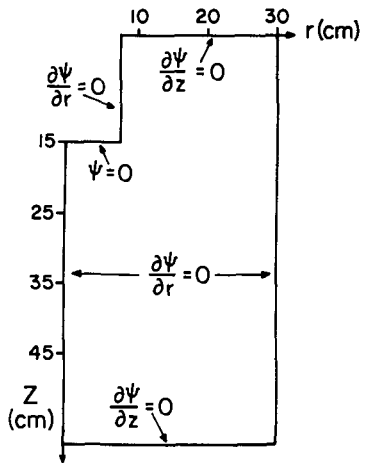

Fig. 3. Schematic cross section and boundary conditions for the furrow irrigation example.

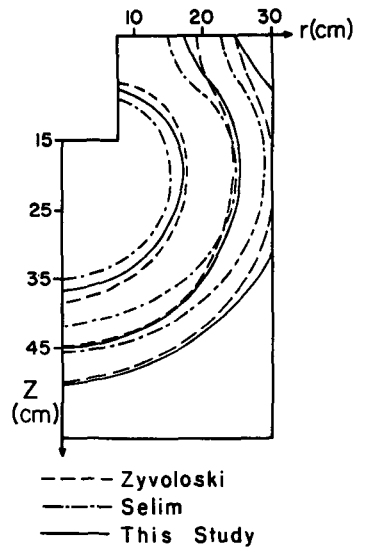

Fig. 4. Comparison of calculated water content distributions for the furrow irrigation problem.

with the results of Zyvoloski et al. (1976) and Selim and Kirkham (1973). Clearly, our results agree closely with those of Zyvoloski et al., but differ from the ADI solution of Selim and Kirkham.

Example 2. The time dependent behavior of the global mass balance often gives a good estimate of the overall accuracy of a numerical solution. Figure 5 and 6 show calculated mass balances for trickle irrigation from a line source using the same rectangular geometry as in Fig. 1. Results in Fig. 5 are for two irrigation rates involving a sandy soil, and assuming a regular grid system with constant nodal spacings of 2 cm. Figure 6 gives similar results for a loess soil, assuming grid spacings of 1 and 2 cm. These examples were previously considered by Ababou (1981), who also gave a detailed description of the unsaturated hydraulic properties of the two soils. No surface ponding occurred for both soil types. Figure 5 shows that mass balance errors for the DEK sand of Ababou became less than about 0.5% after only a few minutes of infiltration. Much larger errors occurred with the MC4 loess soil (Fig. 6), which had a very low saturated hydraulic conductivity; errors in this case remained

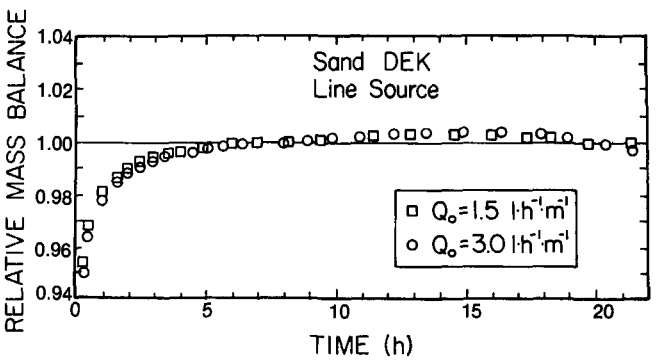

Fig. 5. Calculated mass balance errors during line-source trickle irrigation on DEK sand for two irrigation rates.

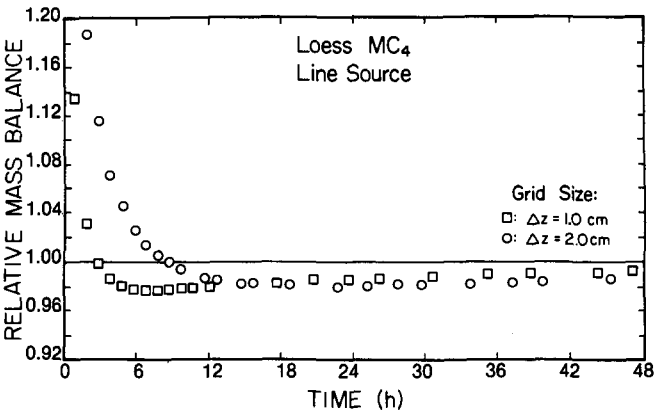

Fig. 6. Calculated mass balance errors during line-source trickle irrigation on a loess soil for two finite difference nodal spacings.

about 2% during the simulation. Improved accuracy in this case was only possible by decreasing the nodal spacing. The errors shown in Fig. 5 and 6 were only about one-fourth of those obtained by Ababou (1981).

Example 3. We briefly present two other cases for trickle irrigation. The first case was carried out for the same loess soil as in Example 2. We again compared our results with those obtained by Ababou (1981) using an ADI-based model. The following experiments were simulated: a line source with discharge rates of 0.5, 1.5, and 3.0 L h^{-1} m^{-1}, and a point source with irrigation rates of 0.5, 1.5, and 3.0 L h^{-1}. An irregular finite difference grid was now used for the calculations; the vertical nodal spacing increased from 2 cm at the soil surface to 4 cm at the lower boundary, while a constant spacing of 2 cm was used in the horizontal direction. The calculated mass balance errors and saturated soil surface areas are summarized in Table 2. Note the large differences in mass balance between our scheme and the ADI scheme of Ababou (1981). Figure 7 shows a typical example of the type of water content distributions obtained for a line source. As for the ponded infiltration case (Example 1), the moisture front calculated with the ADI model is located at a shallower depth than those obtained with our finite difference solution.

Model results were also compared with those obtained by Brandt et al. (1971) for the more fine-textured Gilat loam, which was expected to show much larger discrepancies compared with their Nahal Sinai sand. Simulations were carried out for two trickle discharge rates (0.495 and 0.983 cm^3 cm^{-1} min^{-1}) as used

Table 2. Calculated mass balances and saturated soil surface areas for three trickle irrigation rates involving a line source and a point source. Results of this study are compared with those obtained by Ababou (1981) using an ADI scheme.

	Line source discharge rate Q_0 (L h^{-1} m^{-1})			Point source discharge rate Q_0 (L h^{-1})		
	0.5	1.5	3.0	0.5	1.5	3.0
Mass balance % this study	<1.0	<1.0	<1.0	<1.0	<1.0	<1.0
Mass balance % Ababou (1981)	−3.5	−5.6	−9.8	−3.0	−6.2	−8.6
R_s this study, cm	2.0	23.0	47.5	18.0	39.0	58.0
R_s Ababou (1981), cm	1.5	20.0	46.0	16.0	36.0	53.0

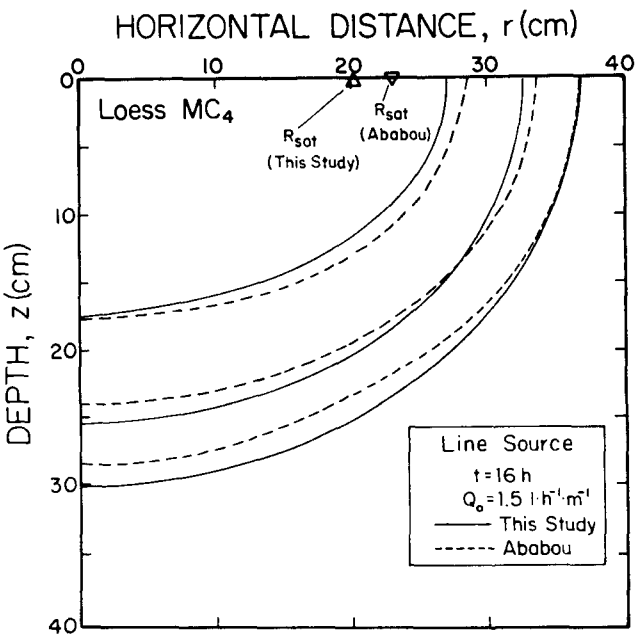

Fig. 7. Calculated water content distributions resulting from line-source trickle irrigation on a loess soil.

by Brandt et al., and assuming plane symmetry. The same irregular finite difference grid as before was applied. We obtained much smaller saturated zones at the soil surface, especially for the higher trickle irrigation rate (Fig. 8). After applying 3 L of water, the model of Brandt et al. yielded saturated areas corresponding to R_s values of 11 and 24 cm for the two discharge rates, while we obtained R_s values of 3 and 9.5 cm, respectively. Water content distributions in the profile were also different, with our calculations showing deeper infiltration of water. Similar but smaller differences between the ADI and finite difference/finite element solutions were already noted in Example 1, as well as in the preceding case involving trickle irrigation.

SUMMARY AND CONCLUSIONS

An improved numerical model for simulating saturated-unsaturated water flow in general and trickle irrigation in particular has been described. The time-dependent nature of the interface between the saturated and unsaturated zones at the soil surface was simulated by means of a moving boundary-type differential equation. This equation was coupled with the unsaturated flow equation through the water flux across the saturated zone at the soil surface. A new and computationally efficient algorithm was used to avoid the calculation of fluxes across the saturated surface area by uncentered finite difference equations. The numerical solution was successfully tested against two other numerical finite difference/finite element solutions for furrow irrigation subject to Dirichlet boundary conditions, and for trickle irrigation involving Neuman-type conditions at the soil surface.

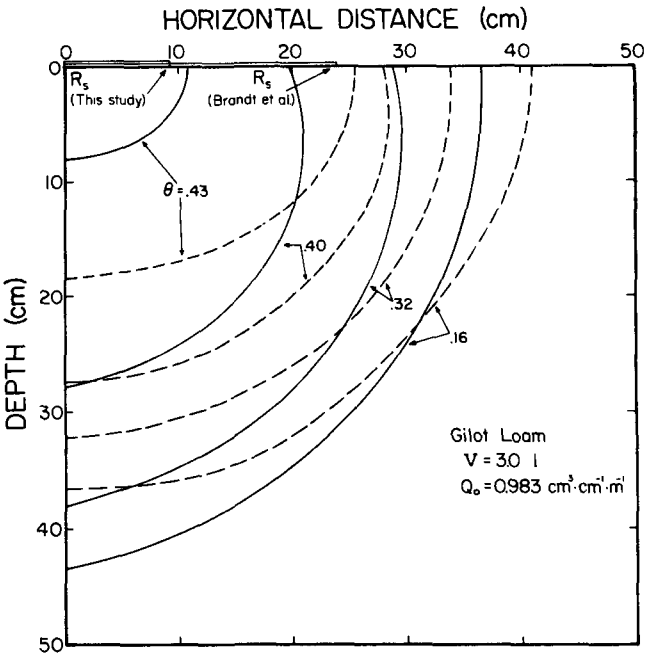

Fig. 8. Calculated water content distributions obtained in this study (solid lines) and by Brandt et al., 1971 (dashed lines) for line-source trickle irrigation on Gilat loam.

We also compared our results with those obtained by Ababou (1981) and Brandt et al. (1971). Comparisons for trickle irrigation involving surface ponding were carried out using various soil hydraulic data sets. Our algorithm for calculating the saturated area at the soil surface produced excellent mass balances as compared with these previous solutions. The algorithm also resulted in improved estimates of the saturated surface area, and in improved predictions of the soil water content in the profile. The numerical solution will be used in Part 2 of this study (Lafolie et al., 1989) to analyze a set of field experiments involving trickle irrigation.

REFERENCES

Ababou, R. 1981. Modélisation des transferts hydriques dans le sol en irrigation localisée. Thesis, Univ. de Grenoble, France.

Ben-Asher, J., D.O. Lomen and A.W. Warrick. 1978. Linear and nonlinear models of infiltration from a point source. Soil Sci. Soc. Am. J. 42:3–6.

Brandt, A., E. Bresler, N. Diner, I. Ben-Asher, J. Heller, and D. Goldberg. 1971. Infiltration from a trickle source, I. Mathematical models. Soil Sci. Soc. Am. Proc. 35:675–682.

Bresler, E., J. Heller, N. Diner, I. Ben-Asher, A. Brandt, and D. Goldberg. 1971. Infiltration from a trickle source, II. Experimental data and theoretical predictions. Soil Sci. Soc. Am. Proc. 35:683–689.

Bucks, D.A., F.S. Nakayama, and A.W. Warrick. 1982. Principles, practices, and potentialities of trickle (drip) irrigation, p. 219–290. *In* D. Hillel (ed.) Advances in infiltration, Vol. 1. Academic

Press, New York.
Caussade, B.H., G. Dournes, and G. Renard. 1979. A new numerical solution of unsteady, two-dimensional flow in unsaturated porous media. Soil Sci. 127:193–201.
Fairweather, G. 1978. Finite element Galerkin methods for differential equations. Dekker, New York.
Firdaouss, A., and T.-P.-Loc. 1983. Infiltration bidimensionelle de l'eau dans les sols non saturés à partir de tranchées rectangulaires équidistantes. Res. Rep. Université d'Orsay, Paris.
Fletcher Armstrong, C., and T.V. Wilson. 1983. Computer model for moisture distribution in stratified soil under a trickle source. Trans. ASAE, 26:1704–1709.
Godounov, S. 1973. Equations de la physique mathématique. Editions MIR, Moscou.
Hillel, D. 1985. Status of research in drip/trickle irrigation. p. 13. *In* Proc. 3rd Int. Drip/Trickle Irrigation Cong., Fresno, CA. 18–21 Nov. 1985. vol. I. ASAE, St. Joseph, MI.
Lafolie, F., R. Guennelon, and M.Th. van Genuchten. 1989. Analysis of water flow under trickle irrigation. I. Theory and numerical solution. Soil Sci. Soc. Am. J. 53:1318–1323 (this issue).
Levin, I., P.C. van Rooyen, and F.C. van Rooyen. 1979. The effect of discharge rate and intermittent water application by point-source irrigation on the soil moisture distribution pattern. Soil Sci. Soc. Am. J. 43:8–16.
Lockington, D., J.-Y. Parlange, and A. Surin. 1983. Optimal prediction of saturation and wetting front during trickle irrigation. Soil Sci. Soc. Am. J. 48:488–494.
Lomen, D.O., and A.W. Warrick. 1974. Time dependent linearized infiltration, II. Line sources. Soil Sci. Soc. Am. Proc. 38:568–572.
Mitchell, A.R., and D.F. Griffith. 1980. The finite difference method in partial differential equations. John Wiley & Sons, New York.
Mostaghimi, S., and J.K. Mitchell. 1983. Pulse trickling effects on soil moisture distribution. Water Resour. Bull. 19:605–612.
Phillip, J.R. 1971. General theorem on steady infiltration from surface sources with application to point and line sources. Soil Sci. Soc. Am. Proc. 35:867–871.
Raats, P.A.C. 1971. Steady infiltration from point sources, cavities, and basins. Soil Sci. Soc. Am. Proc. 35:689–694.
Raats, P.A.C. 1972. Steady infiltration from sources at arbitrary depth. Soil Sci. Soc. Am. Proc. 36:399–401.
Ragab R., J. Feyen, and D. Hillel. 1984. Simulating infiltration in sand from a trickle line source using the matric flux potential concept. Soil Sci. 137:120–127.
Richtmeyer, R.D., and K.W. Morton. 1967. Difference methods for initial values problems. Interscience, New York.
Russo, D., and Bresler, E. 1980. Scaling soil hydraulic properties of a heterogeneous field. Soil Sci. Soc. Am. J. 44:681–684.
Selim, H.M, and D. Kirkham. 1973. Unsteady two-dimensional flow of water in unsaturated soils above an impervious barrier. Soil Sci. Soc. Am. Proc. 37:489–495.
Van der Ploeg, R.R., and P. Benecke. 1974. Unsteady unsaturated, n-dimensional moisture flow in soil: A computer simulation program. Soil Sci. Soc. Am. Proc. 38:881–885.
Vauclin, M., R. Haverkamp, and G. Vachaud. 1979. Résolution numérique d'une équation de diffusion non-linéaire. Presses Univ. de Grenoble, France.
Warrick, A.W. 1974. Time dependent linearized infiltration, I. Point sources. Soil Sci. Soc. Am. Proc. 38:383–386.
Warrick, A.W. 1985. Point and line infiltration. Calculation of the wetted soil surface. Soil Sci. Soc. Am. J. 49:1581–1583.
Warrick, A.W., and D.O. Lomen. 1976. Time dependent linearized infiltration, III. Strip and disc sources. Soil Sci. Soc. Am. J. 40:639–643.
Wooding, R.A. 1968. Steady infiltration from a shallow circular pond. Water Resour. Res. 4:1259–1273.
Zyvoloski, G., J.C. Bruch, and J.M. Sloss. 1976. Solution of equation for two-dimensional infiltration problems. Soil Sci. 122:65–70.